Pergamon

Int. J. Solids Structures Vol. 34, No. 22, pp. 2843–2856, 1997

0020–7683/97 $17.00 + .00

PII: S0020–7683(96)00184–9

AXISYMMETRIC SUBSTITUTE STRUCTURE FOR SCALLOPED DISKS WITH NONCENTRAL HOLES

GUIDO DHONDT
MTU Motoren-und Turbinen-Union München GmbH, Postfach 50 06 40,
80976 München, Germany

(*Received* 27 *November* 1995; *in revised form* 28 *May* 1996)

Abstract—Using the alternating method and the complex function technique of Muskhelishvili the stress field is obtained for a scalloped disk with noncentral holes. Based on this stress field an axisymmetric substitute structure is devised which allows for the determination of the stress concentration factors at holes and scallops without need for a 3-dimensional calculation. The method makes axisymmetric Finite Element calculations of large, predominantly axisymmetric structures such as aircraft engine compressor and turbine disks, in which the non-axisymmetric disturbances are modelled by axisymmetric elements with different material parameters, particularly attractive.
© 1997 Elsevier Science Ltd.

1. INTRODUCTION

In aircraft engine applications one frequently encounters large predominantly axisymmetric structures with local non-axisymmetric disturbances. This situation leads to a difficult dilemma. On the one hand, it is very attractive to perform a 2-dimensional axisymmetric calculation thus avoiding an expensive 3-dimensional analysis. On the other hand, disturbances usually produce stress concentrations which are often very important in subsequent damage calculations. In previous articles (Köhl *et al.*, 1996), an axisymmetric substitute structure was developed which allows for an accurate determination of the concentrated stress at holes. In the present article, the case of a scalloped disk is looked at. Scallops (Fig. 1) are frequently introduced in thin rings with bolt holes to decrease the

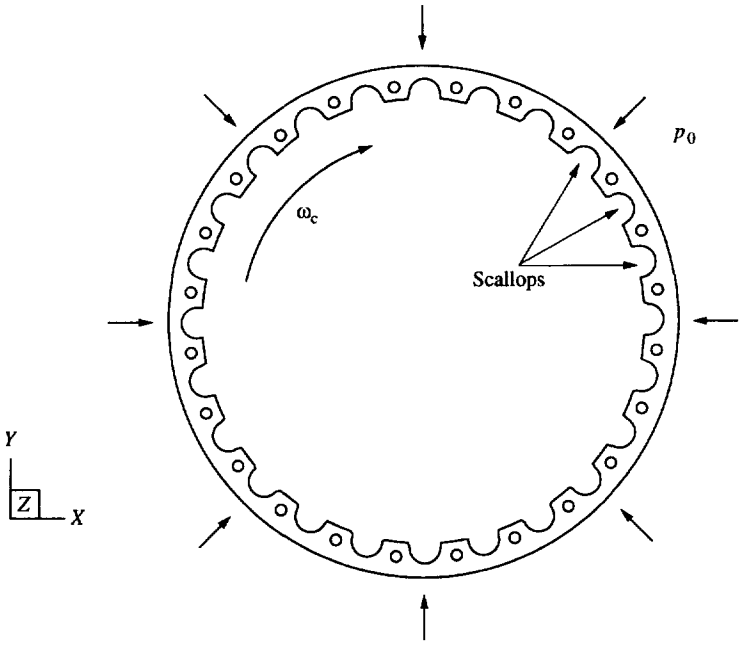

Fig. 1. Scalloped disk with noncentral holes.

stress at the holes. The axisymmetric substitute structure developed yields the local stress at the scallops and the holes.

The first sections of the article deal with the determination of the stress field in the scalloped disk with noncentral holes. The alternating method is used since it is very well suited to analyse topologically similar structures quickly without the need for remeshing like in the Finite Element Method. To this end the stress field outside a scalloped hole in infinite space is developed using a conformal mapping technique (Grassmann, 1979) and the complex function theory of Muskhelishvili (1953). A comparison with a Finite Element Calculation shows good agreement. Finally, a suitable axisymmetric substitute structure is developed and the appropriate parameters are determined.

2. ITERATIVE CALCULATION OF STRESSES IN SCALLOPED DISKS WITH NONCENTRAL HOLES

In order to find the stresses in a scalloped disk with noncentral holes subject to centrifugal forces and outer pressure (Fig. 1), the so-called alternating technique will be applied. The basic idea of this method is to find a solution to the governing equations at stake satisfying only part of the boundary conditions. This should be an easier task than the original one. Next, another solution to the governing equations is superimposed making sure that the boundary conditions which were not yet satisfied are fulfilled. However, this latter solution usually destroys the fulfilment of the boundary conditions which were satisfied by the first solution. So the first solution must be applied again. This procedure is repeated until a convergent solution is obtained. It is often advantageous to alternate more than two solutions.

For the scalloped disk with noncentral holes the solution of the disk without holes and scallops subject to centrifugal forces and outer pressure will be taken as the starting solution. Analytical expressions for this starting solution are given by Timoshenko (1970).

At this point the first iteration starts. The starting solution leads to stresses on the surface of the noncentral holes. Since these should be stress-free, the inverse stress must be applied. For the determination of the stress fields in the disk due to the application of the inverse stresses at just one hole, the solution of the hole problem in infinite space with arbitrary loading, given by Muskhelishvili (Muskhelishvili, 1953, Köhl *et al.*, 1996) is taken. Application of this solution to the first noncentral hole frees this hole from all stress. However, it leads to additional stresses at all other noncentral holes and at the inner and outer boundary of the disk. This procedure is repeated for all noncentral holes. At this stage the boundary conditions at the inner surface, which are not satisfied due to the noncentral hole stress fields and the starting solution in the scallops, are restored by superimposing the stresses around a scalloped boundary in infinite space loaded by the inverse stress fields. The solution to this problem is derived in Sections 4–6 of the present article. Finally, the outer surface is freed from the noncentral holes and scalloped boundary stress fields. The solution to this problem was obtained by Muskhelishvili (1953) and is reproduced in Section 3. At this point the second iteration can start. This procedure is repeated until convergence for the stress fields is reached.

3. SOLUTION TO THE PROBLEM OF A CIRCULAR DISK WITH ARBITRARY LOADING

The center of the coordinate axes coincides with the center of the disk and an arbitrary point is denoted by the complex number $z = x+\mathrm{i}y$. R is the radius of the disk and θ the counter clockwise angular coordinate. Let $(t_x(\theta), t_y(\theta))$ be the stress vector at position θ, and let the resultant force defined by

$$f_1(\theta)+\mathrm{i}f_2(\theta) := \mathrm{i}R\int_0^\theta (t_x(\xi)+\mathrm{i}t_y(\xi))\,\mathrm{d}\xi \tag{1}$$

where $\theta = 0$ is some position along the boundary, be expressed in a Fourier series

$$f_1(\theta)+if_2(\theta) = \sum_{-\infty}^{\infty} A_n e^{in\theta} \tag{2}$$

then the stress field at z, an arbitrary point inside the disk, satisfies:

$$\begin{aligned} \sigma_{xx}+\sigma_{yy} &= 2[\Phi(z)+\overline{\Phi(z)}] \\ \sigma_{yy}-\sigma_{xx}+2i\sigma_{xy} &= 2[\bar{z}\Phi'(z)+\Psi(z)] \end{aligned} \tag{3}$$

where Φ and Ψ are two potentials, $'$ denotes the derivative with respect to z and a bar denotes the complex conjugate. The potentials take the form (Muskhelishvili, 1953):

$$\Phi(z) = \frac{d\phi}{dz} \tag{4}$$

$$\Psi(z) = \frac{d\psi(z)}{dz} \tag{5}$$

where

$$\phi(z) = \sum_{k=1}^{\infty} a_k z^k \tag{6}$$

$$\psi(z) = \sum_{k=0}^{\infty} b_k z^k \tag{7}$$

and

$$a_1 = \frac{A_1}{2R} \tag{8}$$

$$a_n = \frac{A_n}{R^n}, \quad n \geqslant 2 \tag{9}$$

$$b_n = \frac{\bar{A}_{-n}}{R^n} - (n+2)\frac{A_{n+2}}{R^n}, \quad n \geqslant 0. \tag{10}$$

4. CONFORMAL MAPPING FOR A SCALLOPED BOUNDARY

The problem of finding the stress field in infinite space due to an arbitrary loading along a scalloped hole will be found by mapping the space around the scalloped hole onto the inside of the unit circle. Taking the smallest radius along the scalloped hole as the unit

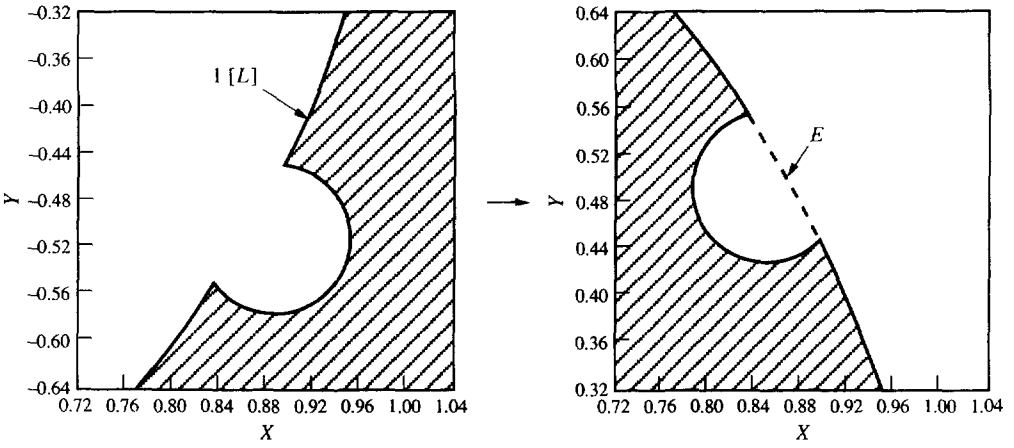

Fig. 2. Mapping the exterior of a scalloped hole in infinite space into the unit circle.

of length $[L]$ and applying the inverse transformation

$$\xi = \frac{1}{z} \tag{11}$$

maps the exterior of the scalloped hole into the unit circle E (Fig. 2). To map the latter domain onto E, Grassmann (1979) has described a suitable mapping algorithm using the method of successive approximation. His algorithm consists of three routines, the circle routine, the ray routine and the Koebe routine, of which only the first one will be needed here. Repeated application of the routines produces a domain more and more similar to E. Assume the boundary of the domain to be mapped is defined by n boundary points $z_1, \ldots, z_n \in \mathbb{C}$, in counter clockwise direction. Let z_i (Fig. 3) be such that

$$|z_i| \leqslant |z_j|, \quad j = 1, \ldots, n \tag{12}$$

and the preceding point be expressed by z_{i-1} (set $z_{i-1} = z_n$ for $i = 1$).

Defining $F_j^i := (z_j - z_i)/(z_j - z_{i-1})$, let m be such that

$$\operatorname{Im}[F_m^i/|F_m^i|] := \min_{\substack{j=1,\ldots,n \\ j\neq i \\ j\neq i-1}} \{\operatorname{Im}[F_j^i/|F_j^i|]\} \tag{13}$$

where Im denotes the imaginary part. Then, using the abbreviation $A := F_m^i/|F_m^i|$,

$$R_k = \tfrac{1}{2}|z_i - z_{i-1}|/|\operatorname{Im} A| \tag{14}$$

and

$$C_k = \frac{1}{2}\left[z_i + z_{i-1} + i(z_i - z_{i-1})\frac{\operatorname{Re} A}{\operatorname{Im} A}\right] \tag{15}$$

are radius and center, respectively, of a circle K_k passing through z_i and z_{i-1} and one more of the boundary points without intersecting the domain at stake, i.e., either $E \cap K_k$ or $E \backslash K_k$ can be chopped off (Re denotes the real part of a complex argument, the index k denotes the iteration). In the present application $E \cap K_k$ will be chopped off. To this end the domain is first rotated so that the center of K_k lies on the real axis with the part to be chopped off on the left. This is performed by the transformation

$$f_k(z) = z \cdot D_k \tag{16}$$

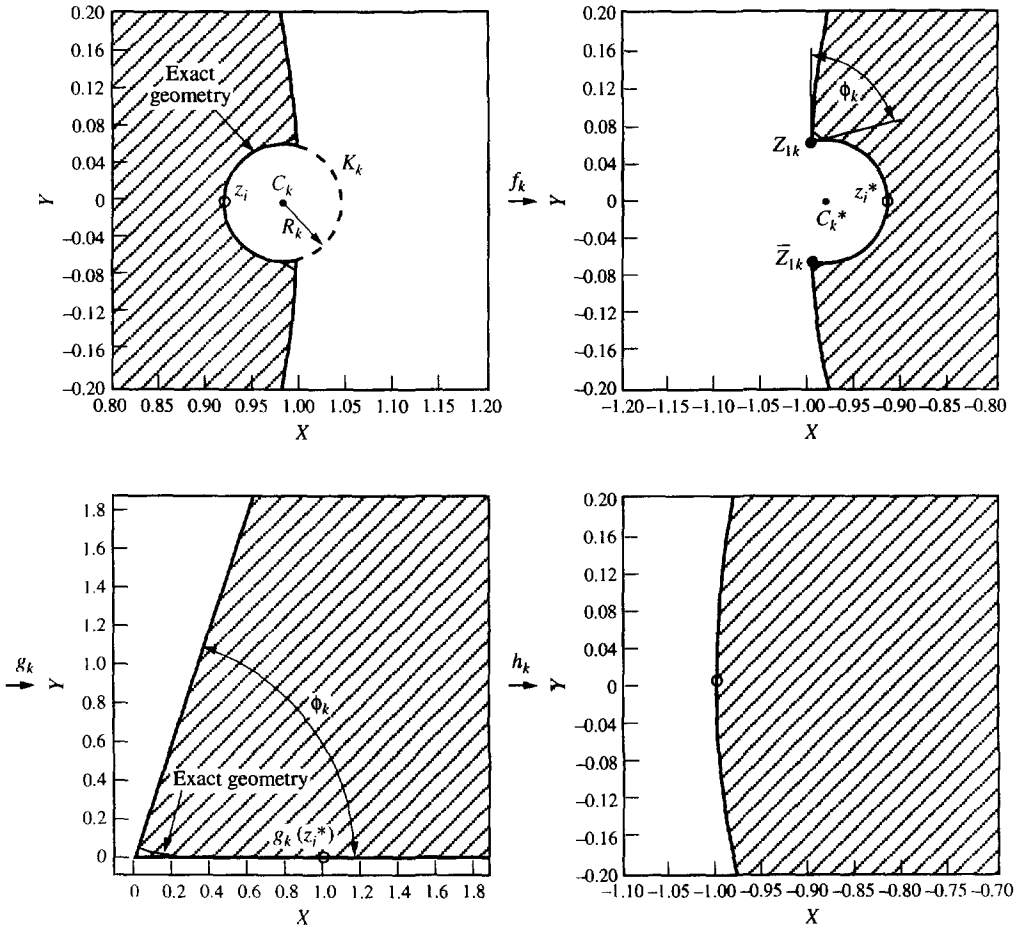

Fig. 3. Conformal transformation $T_k(z)$ of one scallop.

where

$$D_k = \operatorname{sgn}(\operatorname{Im} A) \cdot \frac{\bar{C}_k}{|C_k|} \tag{17}$$

sgn denotes the sign of a real number. If K_k intersects the unit circle in two distinct points these take the form Z_{1k} and $\bar{Z}_{1k}$ where

$$\operatorname{Re} Z_{1k} = \frac{[(C_k^* + R_k)(C_k^* - R_k) + 1]}{2C_k^*} \tag{18}$$

$$\operatorname{Im} Z_{1k} = \sqrt{1 - (Re Z_{1k})^2}, \tag{19}$$

$C_k^* = C_k \cdot D_k$. In our application this is the case. If this condition is not satisfied the ray and Koebe routine must be taken. This generally occurs when the domain exhibits deep inlets with locally small radii of curvature. $E \backslash K_k$ is mapped onto a wedge shape by

$$g_k(z) = \frac{z - Z_{1k}}{z - \bar{Z}_{1k}} A_k \tag{20}$$

where

$$A_k = \frac{z_i^* - \bar{Z}_{1k}}{z_i^* - Z_{1k}}, \tag{21}$$

$z_i^* = z_i \cdot D_k$ (Fig. 3). The angle ϕ_k of the wedge satisfies

$$\phi_k = \left| \arg\left(\frac{Z_{1k} - C_k^*}{Z_{1k}} \right) \right| \tag{22}$$

arg denotes the argument of a complex number. Finally the wedge shape is mapped onto the unit circle by

$$h_k(z) = \frac{z^{\pi/\phi_k} - B_k}{z^{\pi/\phi_k} - \bar{B}_k} \cdot C_k \tag{23}$$

where

$$B_k = g_k(0)^{\pi/\phi_k} \tag{24}$$

$$C_k = \frac{g_k(1)^{\pi/\phi_k} - \overline{g_k(0)^{\pi/\phi_k}}}{g_k(1)^{\pi/\phi_k} - g_k(0)^{\pi/\phi_k}}. \tag{25}$$

The complete mapping T_k is obtained by combining eqns (16), (20) and (23):

$$\zeta = T_k(z) = h_k \circ g_k \circ f_k(z). \tag{26}$$

In general, several such mappings (characterized by the index k) will be needed to obtain a satisfactory approximation of the unit circle.

In what follows the inverse transformation will be needed:

$$z = T_k^{-1}(\zeta) = f_k^{-1} \circ g_k^{-1} \circ h_k^{-1}(\zeta) \tag{27}$$

where

$$f_k^{-1}(\zeta) = \frac{\zeta}{D_k} \tag{28}$$

$$g_k^{-1}(\zeta) = \frac{\bar{Z}_{1k}\zeta - Z_{1k}A_k}{\zeta - A_k} \tag{29}$$

$$h_k^{-1}(\zeta) = \left[\frac{\bar{B}_k\zeta - B_kC_k}{\zeta - C_k} \right]^{\phi_k/\pi}. \tag{30}$$

Note that h_k^{-1} has a branch point for a zero numerator and a zero denominator, i.e., for

$$\zeta = C_k \tag{31}$$

and

$$\zeta = C_k \frac{B_k}{\bar{B}_k}. \tag{32}$$

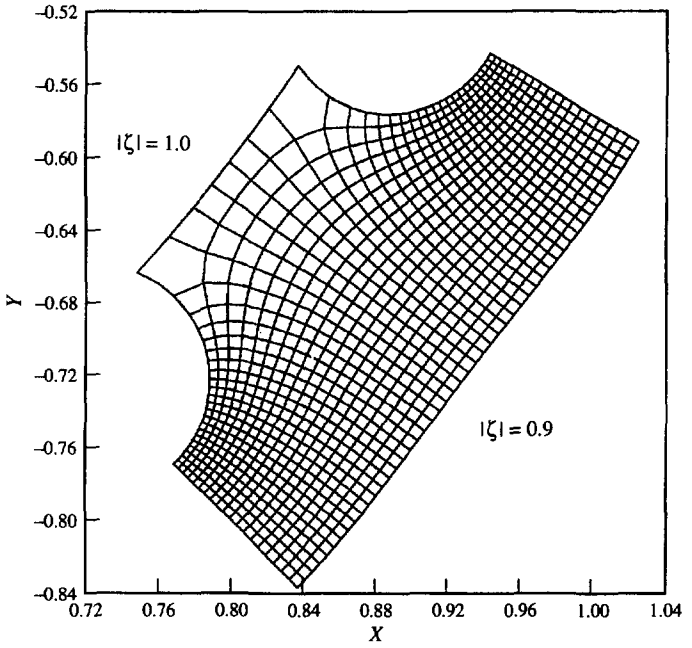

Fig. 4. Conformal mapping $\omega(\zeta)$.

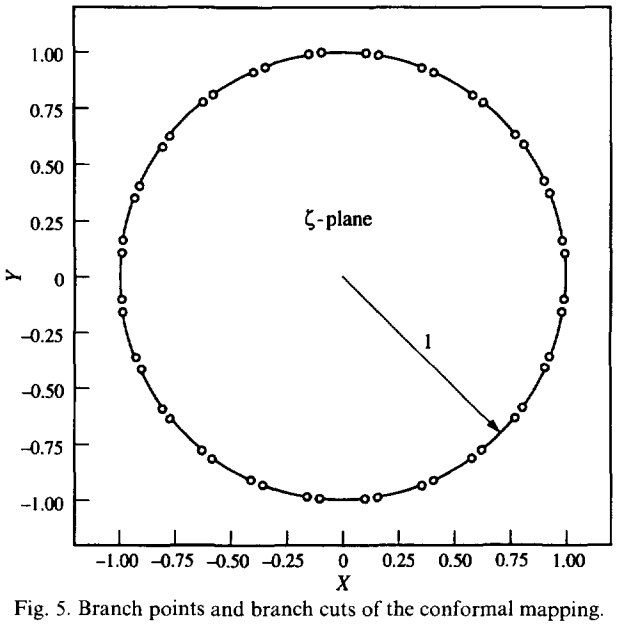

Fig. 5. Branch points and branch cuts of the conformal mapping.

Both branch points lie on the unit circle. Repeated application of the above algorithm finally leads to the conformal mapping $\omega(\zeta)$:

$$\omega(\zeta) = [\ldots T_3^{-1}(\zeta) \circ T_2^{-1}(\zeta) \circ T_1^{-1}(\zeta)]^{-1}. \tag{33}$$

The exponent -1 finds its origin in eqn (11). For the geometry in Fig. 1 only one transformation per scallop was needed to yield satisfactory results. The complete conformal mapping is shown in Fig. 4, where iso-$|\zeta|$ and iso-$(\arg\zeta)$ lines are shown. Although the geometry deviates slightly from the original design for $|z| = 1$, the critical areas ahead of the scallops are very well matched. Figure 5 shows the location of the branch points for a geometry with 24 scallops.

5. SOLUTION FOR THE POTENTIAL FUNCTIONS

In carthesian coordinates the stresses can be expressed in terms of potential functions $\phi(z)$ and $\psi(z)$ by eqns (3)–(5). The boundary conditions reduce to (Muskhelishvili, 1953):

$$\phi(z)+z\overline{\Phi(z)}+\overline{\psi(z)} = \text{if}+\text{constant} \tag{34}$$

where

$$f = \int_0^s (t_x+\mathrm{i}t_y)\,\mathrm{d}s \tag{35}$$

s is an arc coordinate along the boundary and (t_x, t_y) are the stress components in carthesian coordinates. If a conformal mapping is used $\phi(z)$ and $\psi(z)$ are expressed as a function of ζ, i.e. (Chiu and Gao, 1993):

$$\phi(\zeta) = \phi(\omega^{-1}(z)) \tag{36}$$

$$\psi(\zeta) = \psi(\omega^{-1}(z)). \tag{37}$$

For convenience the same symbols for the complex potentials in the ζ-plane are used. Now eqns (3)–(5) are transformed into:

$$\Phi(\zeta) = \frac{\mathrm{d}\phi(z)}{\mathrm{d}z} = \frac{1}{\omega'(\zeta)}\frac{\mathrm{d}\phi(\zeta)}{\mathrm{d}\zeta} \tag{38}$$

$$\Psi(\zeta) = \frac{1}{\omega'(\zeta)}\frac{\mathrm{d}\psi(\zeta)}{\mathrm{d}\zeta} \tag{39}$$

$$\sigma_{xx}+\sigma_{yy} = 2[\Phi(\zeta)+\overline{\Phi(\zeta)}] \tag{40}$$

$$\sigma_{yy}-\sigma_{xx}+2\mathrm{i}\sigma_{xy} = \frac{2}{\omega'(\zeta)}[\overline{\omega(\zeta)}\Phi'(\zeta)+\omega'(\zeta)\Psi(\zeta)] \tag{41}$$

where

$$' := \frac{\mathrm{d}}{\mathrm{d}\zeta}. \tag{42}$$

The boundary condition (34) is transformed into

$$\phi(\sigma)+\omega(\sigma)\frac{\overline{\phi'(\sigma)}}{\overline{\omega'(\sigma)}}+\overline{\psi(\sigma)} = \text{if}+\text{constant} \tag{43}$$

where $\zeta = \sigma$ was written on the boundary. In the present application the ζ-domain is E and its boundary is the unit circle. The solution $\phi(\zeta)$ and $\psi(\zeta)$ will be assumed to be holomorphic for $|\zeta| < 1$ and continuous up to $|\zeta| = 1$. Then functions $\phi^*(\zeta)$ and $\psi^*(\zeta)$ can be defined which are holomorphic for $|\zeta| > 1$ and continuous up to $|\zeta| = 1$ by:

$$\phi^*(\zeta) := \bar{\phi}\left(\frac{1}{\zeta}\right) := \overline{\phi\left(\frac{1}{\bar{\zeta}}\right)} \tag{44}$$

and similarly for ψ. Since on the unit circle

$$\bar{\sigma} = \frac{1}{\sigma}. \tag{45}$$

Equation (43) can be rewritten in the form

$$\phi(\sigma) + \omega(\sigma)\frac{\bar{\phi}'\left(\frac{1}{\sigma}\right)}{\bar{\omega}'\left(\frac{1}{\sigma}\right)} + \bar{\psi}\left(\frac{1}{\sigma}\right) = \sum_{k=-\infty}^{-1} a_k\sigma^k + \sum_{k=0}^{\infty} a_k\sigma^k. \tag{46}$$

The right hand side was expanded in a Fourier series (on the unit circle the Laurent series expansion and Fourier series expansion coincide since $\sigma = e^{i\theta}$). Now a theorem states that if a function $A(\zeta)$ is holomorphic for $|\zeta| < 1$, if $B(\zeta)$ is holomorphic for $|\zeta| > 1$ (including the point at infinity), if both functions are continuous up to $|\zeta| = 1$ and if

$$A(\zeta) + B(\zeta) = 0, |\zeta| = 1 \tag{47}$$

then $A(\zeta) = \text{constant} = -B(\zeta)$ (Muskhelishvili, 1953).

Applying this to eqn (46) it is clear from the above that the first term on the left hand side and the last term on the right hand side are holomorphic for $|\zeta| < 1$ whereas the last term on the left hand side and the first term on the right hand side are holomorphic for $|\zeta| > 1$. The second term on the left hand side is a mixed term. Moreover, it contains the derivation of the conformal mapping, which is not continuous on $|\zeta| = 1$.

This problem is resolved by assuming that $\phi'(\sigma)$ removes the discontinuity in $1/\omega'(\sigma)$. This is a reasonable assumption, since these are the only terms in eqn (46) for which a discontinuity on $|\zeta| = 1$ occurs (or can occur). The following expansion is proposed:

$$\Phi(\zeta) = \frac{\phi'(\zeta)}{\omega'(\zeta)} = \sum_{m=1}^{\infty} b_m\zeta^{m+1}. \tag{48}$$

Note that the lowest order term is quadratic in order to ensure the right asymptotic behaviour for $\zeta \to 0$. Indeed, since

$$\omega(\zeta) \sim \frac{1}{\zeta}, \quad \zeta \to 0 \tag{49}$$

(the exterior of the scalloped boundary is mapped onto the interior of the unit circle) one obtains

$$\Phi(\zeta) \sim \zeta^2, \quad \zeta \to 0. \tag{50}$$

This ensures the right far field behaviour for the stresses. Equation (48) leads to:

$$\phi(\sigma) = \sum_{m=1}^{\infty} b_m \int_{\sigma_0}^{\sigma} \omega'(\xi)\xi^{m+1}\,\mathrm{d}\xi = \sum_{k=0}^{\infty}\left[\sum_{m=1}^{\infty} b_m d_{km}\right]\sigma^k \tag{51}$$

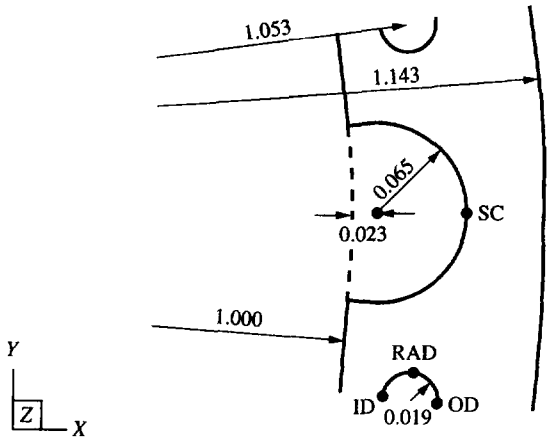

Fig. 6. Example geometry.

where

$$\int_{\sigma_o}^{\sigma} \omega'(\xi)\xi^{m+1}\,\mathrm{d}\xi = \sum_{k=0}^{\infty} d_{km}\sigma^k \tag{52}$$

is obtained by an ordinary Fourier expansion. Using eqn (48) again, the second term in eqn (46) yields

$$\omega(\sigma)\frac{\overline{\phi'(\sigma)}}{\overline{\omega'(\sigma)}} = \sum_{m=1}^{\infty} \bar{b}_m[\omega(\sigma)\cdot\sigma^{-1-m}] = \sum_{k=-\infty}^{\infty}\left[\sum_{m=1}^{\infty} \bar{b}_m c_{km}\right]\sigma^k \tag{53}$$

where c_{km} is obtained by the following Fourier expansion:

$$\omega(\sigma)\sigma^{-1-m} = \sum_{k=-\infty}^{\infty} c_{km}\sigma^k. \tag{54}$$

Substitution of eqns (51) and (53) into eqn (46) and splitting the contributions which are holomorphic for $|\zeta| < 1$ and $|\zeta| > 1$ yields:

$$\sum_{m=1}^{\infty} b_m d_{km} + \sum_{m=1}^{\infty} \bar{b}_m c_{km} = a_k \quad k = 1, 2, 3, \ldots \tag{55}$$

$$\psi(\sigma) = \sum_{k=1}^{\infty}\left[\bar{a}_{-k} - \sum_{m=1}^{\infty} b_m \bar{c}_{-km}\right]\sigma^k. \tag{56}$$

Equation (55) represents a linear set of infinitely many equations. Taking the first n equations yields $b_1, b_2, \ldots b_n$. Substituting this set into eqns (48) and (56) yields $\Phi(\zeta)$ and $\psi(\zeta)$. The stresses are obtained by eqns (39)–(41).

6. APPLICATION

The alternating method using the solutions of the preceding sections was applied to the disk with scallops and holes in Fig. 6. The inner radius was taken as the unit of length. The material and loading data correspond to typical data for a titanium alloy compressor part at take-off. The stresses are scaled by the hoop stress at the inner radius of a disk with similar dimensions as the original structure but without holes and scallops, subject to

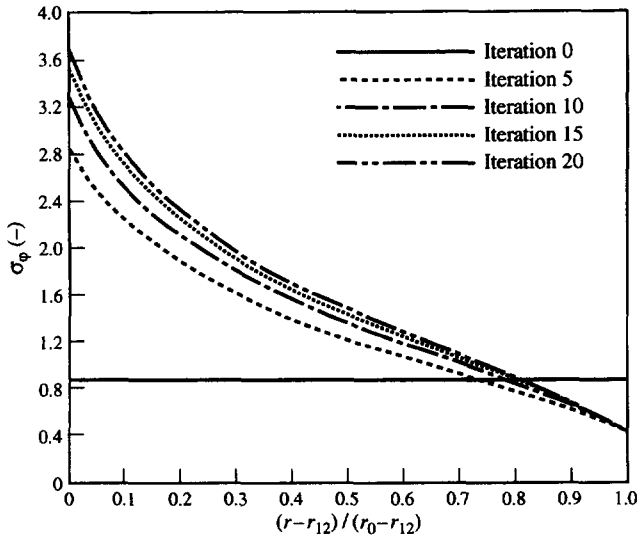

Fig. 7. Hoop stress ahead of the scallop.

centrifugal loading only. Figure 7 shows the hoop stress ahead of the scallops for several iterations. r_o denotes the outer radius, r is the radial coordinate and r_{12} is the maximum value of r along a scallop. It is observed that the method converges slowly towards a limit function. The slow convergence can be explained by the small thickness of the disk: the several solutions used in the alternating method have little space at their disposal to die out, i.e. there is a lot of interaction between the holes, scallops and outer boundary.

Table 1 shows the stresses computed by the alternating method (AM) at selected locations indicated in Fig. 6, together with the deviation δ from Finite Element results (FE) defined as

$$\delta = \frac{\sigma(AM) - \sigma(FE)}{\sigma_{\varphi sc}(FE)} (\%) \tag{57}$$

p_o is the outer pressure. The inner pressure p_i was assumed to be zero. $\bar{\sigma}_\varphi$ at the outside boundary denotes the mean value of the hoop stress along the boundary. The Finite Element results were obtained by using the commercial Finite Element program ABAQUS. Due to symmetry conditions only a segment of the disk enclosing an angle of $\pi/24$ was modelled, using 8-node isoparametric elements. A coarse mesh containing 96 elements and a fine mesh containing 184 elements were generated. Comparison of the stresses in the fine and coarse model yielded deviations below 1%. For the comparison with the alternating method the fine mesh results were used.

There is a good correspondence between the FE and AM results, especially for high stress values. The alternating method yields the advantage that geometrical changes can be quickly taken into account without the need for remeshing. This will generally outweigh the slow convergence noticed in the present example. Indeed, computer cost is very low, i.e., it does not require much cost and effort to include a few more iterations. On the other hand, remeshing frequently involves expensive engineering time. Furthermore, it is expected that convergence is substantially faster for structures which are not so thin.

Table 1. Stresses at selected locations

	SC		ID		RAD		OD		Outside boundary	
p_o [MPa]	σ_φ [—]	δ [%]	σ_φ [—]	δ [%]	σ_r [—]	δ [%]	σ_φ [—]	δ [%]	$\bar{\sigma}_\varphi$ [—]	δ [%]
0	3.714	0.1	0.790	2.6	−0.355	−0.2	1.722	−0.8	1.333	−1.6
20	2.342	3.0	0.488	3.0	−0.249	−1.8	1.061	−1.5	0.817	−1.4

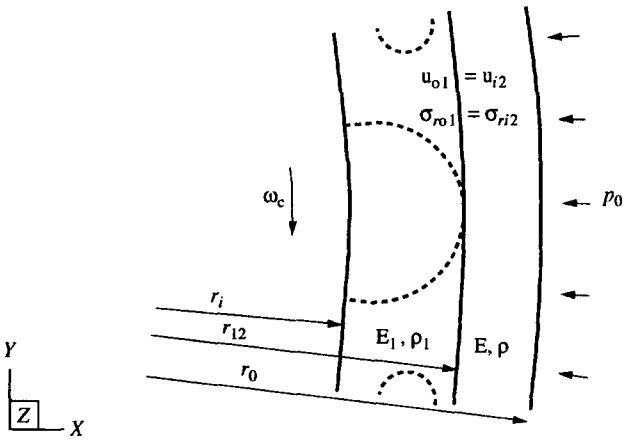

Fig. 8. Axisymmetric substitute structure for the scalloped disk.

7. AXISYMMETRIC SUBSTITUTE STRUCTURE

The scalloped region in Fig. 1 is generally a part of a larger structure, e.g., an aircraft engine compressor containing several stages. The inherent axisymmetry of such structures is usually only locally disturbed by, e.g., holes, scallops or blades. It is therefore natural to investigate whether an expensive three-dimensional calculation can be avoided by replacing the disturbances by axisymmetric substitute structures. In this way the stresses in the original structure can be determined by means of a relatively cheap two-dimensional axisymmetric calculation. The stress concentrations at the local disturbances are taken into account by appropriate stress concentration factors.

For the scalloped disk of Fig. 1 a substitute structure consisting of two rings (Fig. 8) is proposed, in which the scalloped area in the original structure is substituted by an inner ring with a different density and E-modulus. These parameters are determined so that they yield the same radial displacement and radial stress or equivalently the same radial and hoop stress at the outer boundary r_o due to the given load as in the original structure, i.e., the far field solution in the original and substitute structure is the same. The outer boundary is assumed to be far enough from the scalloped area so that no shear stresses occur at $r = r_o$.

Assume the stresses were calculated in the original structure for a given ω_c and p_o, i.e., at $r = r_o$ the hoop stress σ_{to2} and radial stress $\sigma_{ro2} = -p_o$ were obtained. "o" denotes the outer boundary of a ring, "i" the inner boundary. σ_{to2} is linear in ω_c^2 and p_o ($p_i = 0$).

$$\sigma_{to2} = a_1\omega_c^2 + b_1 p_o. \tag{58}$$

Using σ_{ro2} and σ_{to2} as boundary conditions for the substitute structure the stresses and radial displacement on the inside of ring 2 can be determined (Köhl *et al.*, 1996):

$$\sigma_{ri2} = -\frac{r_o^2 - r_{12}^2}{2r_{12}^2}\left[\sigma_{to2} - \frac{r_o^2 + r_{12}^2}{r_o^2 - r_{12}^2}\sigma_{ro2} - \frac{3+\nu}{4}\rho\omega_c^2\left(r_{12}^2 + \frac{1-\nu}{3+\nu}r_o^2\right)\right] \tag{59}$$

$$\sigma_{ti2} = \frac{r_o^2 + r_{12}^2}{2r_{12}^2}\sigma_{to2} - \frac{r_0^2 - r_{12}^2}{2r_{12}^2}\sigma_{ro2} + \frac{3+\nu}{8}\rho\omega_c^2\left[r_o^2 - r_{12}^2 - \frac{1-\nu}{3+\nu}\cdot\frac{r_o^2(r_o^2 + r_{12}^2) - 2r_{12}^4}{2r_{12}^2}\right] \tag{60}$$

$$u_{i2} = \frac{r_{12}}{E}(\sigma_{ti2} - \nu\sigma_{ri2}). \tag{61}$$

Equations (59) and (61) exhibit again a linear relationship in ω_c^2 and p_o:

$$\sigma_{ri2} = a_2\omega_c^2 + b_2 p_o \tag{62}$$

$$u_{i2} = a_3\omega_c^2 + b_3 p_o. \tag{63}$$

The boundary conditions between ring 1 and 2 amount to:

$$\sigma_{ro1} = \sigma_{ri2} \tag{64}$$

$$u_{o1} = u_{i2}. \tag{65}$$

On the other hand, the knowledge of σ_{ro1}, $\sigma_{ri1} = p_i = 0$ and ω_c allows for the calculation of u_{o1} using the material data of ring 1. Reordering this relationship yields a linear equation in E_1 and ρ_1:

$$E_1[u_{o1}] - \rho_1\left[r_{12}\frac{3+\nu}{4}\omega_c^2\left(r_i^2 + \frac{1-\nu}{3+\nu}r_{12}^2\right)\right] = r_{12}\left[\frac{r_{12}^2 + r_i^2}{r_{12}^2 - r_i^2} - \nu\right]\sigma_{ro1}. \tag{66}$$

Substitution of eqns (62)–(65) into eqn (66) yields a relationship of the form:

$$E_1(a_3\omega_c^2 + b_3 p_o) + \rho_1 a_4\omega_c^2 = a_5\omega_c^2 + b_5 p_o. \tag{67}$$

In the above derivation all quantities a_i and b_i are load independent (they depend on the geometry and material constants only). Equation (67) is the relation which has to be satisfied by the material parameters E_1 and ρ_1 of the substitute structure in order to get the same far field solution (σ_{ro2} and σ_{to2}) as in the original structure, both structures being loaded by ω_c and p_o. It is a linear equation in the two unknowns E_1 and ρ_1 and can be satisfied in infinitely many ways for given ω_c and p_o. However, if E_1 and ρ_1 are to be load independent, both the coefficients of ω_c^2 and p_o must vanish. This leads to a set of two equations in the two unknowns E_1 and ρ_1:

$$\begin{aligned} a_3 E_1 + a_4\rho_1 &= a_5 \\ b_3 E_1 &= b_5. \end{aligned} \tag{68}$$

This means that it is generally possible to find an E_1 and ρ_1 so that the required equivalence between the original and substitute structure at $r = r_o$ is always satisfied, independent of the loading (ω_c and p_o)! In practice, calculations are made for two different loadings leading to two equations of the form (66) from which ρ_1 and E_1 are determined.

In this way the scallops and holes of the structure in Fig. 1 are replaced by an axisymmetric substitute structure. Although the substitute structure was designed so that the stress and displacement fields are not changed far enough away, they clearly are very different close to the disturbances. Since disturbances frequently lead to stress concentrations it is still very important to get a precise idea of the stress field in adjacent areas such as the ones indicated by SC, OD, RAD and ID in Fig. 6. This will be achieved by establishing a relationship between these concentrated stresses and the stresses obtained in the substitute structure at a location adjacent to the strongest disturbance, i.e., σ_{ri2} and σ_{ti2} in the present case. The concentrated stresses σ_c in the original structure satisfy an equation of the form

$$\sigma_c = a_6\omega_c^2 + b_6 p_o \tag{69}$$

Table 2. Stress concentration factors at selected locations

	K_t	K_r
$\sigma_{\varphi SC}$	2.58	−3.14
$\sigma_{\varphi ID}$	0.55	0.005
$\sigma_{\varphi OD}$	1.22	0.17
σ_{rRAD}	−0.225	1.92

whereas eqn (60) yields

$$\sigma_{ti2} = a_7\omega_c^2 + b_7 p_o. \tag{70}$$

Together with eqn (62), eqn (70) leads to

$$\omega_c^2 = a_8\sigma_{ti2} + b_8\sigma_{ri2} \tag{71}$$

$$p_o = a_9\sigma_{ti2} + b_9\sigma_{ri2}. \tag{72}$$

Substitution in eqn (69) yields

$$\sigma_c = K_t\sigma_{ti2} + K_r\sigma_{ri2}. \tag{73}$$

So there is a linear relationship between the concentrated stress in the original structure and the stresses σ_{ti2} and σ_{ri2} in the substitute structure. Since all quantities $a_6 \ldots b_9$ are load independent, K_t and K_r do not depend on the load either. In practice, the coefficients in eqn (73) are determined by performing a stress calculation for two different loadings and solving the resultant set of equations.

For the structure in Fig. 6, $E_1/E = 0.153$ and $\rho_1/\rho = 0.52$ was found, i.e., the mass in the scalloped ring is reduced by 2 and the stiffness by 6. The stress concentration factors at several positions are summarized in Table 2. These factors allow for the calculation of the concentrated stresses for an arbitrary loading based on the stresses σ_{ti2} and σ_{ri2} in the substitute structure.

8. CONCLUSIONS

By means of the alternating method the stress fields in a scalloped disk with noncentral holes were obtained. A comparison with Finite Element results showed good agreement. An axisymmetric substitute structure allows for an axisymmetric treatment of large predominantly axisymmetric structures with local disturbances while retaining good accuracy for the concentrated stresses adjacent to the disturbances.

REFERENCES

Chiu, C.-H. and Gao, H. (1993). Stress singularities along a cylcoid rough surface. *International Journal of Solids and Structures* **30,** 2983–3012.

Grassmann, E. (1979). Numerical experiments with a method of successive approximation for conformal mapping. *ZAMP* **30,** 873–884.

Köhl, M., Dhondt, G. and Broede, J. (1996). Axisymmetric substitute structures for circular disks with noncentral holes. *Computers and Structures* **60,** 1047–1065.

Muskhelishvili, N. I. (1953). *Some Basic Problems of the Mathematical Theory of Elasticity*, P. Noordhoff Ltd, Groningen-Holland.

Timoshenko, S. P. and Goodier, J. N. (1970). *Theory of Elasticity*, 3rd edition, McGraw-Hill Kogakusha, Tokyo.